Opto-Electronic Advances

Supplementary information

2018, Vol. 1, No. 1

DOI: 10.29026/oea.2018.170001

Remote-mode microsphere nano-imaging: new boundaries for optical microscope

Lian-Wei Chen, Yan Zhou, Meng-Xue Wu and Ming-Hui Hong*

Department of Electrical and Computer Engineering, National University of Singapore, Engineering Drive 3, Singapore 117576, Singapore
* Correspondence: M H Hong, E-mail: elehmh@nus.edu.sg

This file includes:

Supplementary information is available for this paper at https://doi.org/10.29026/oea.2018.170001

Section 1: Comparison of the imaging techniques from biological aspects[1,2]

Remote-mode microsphere nanoscope can observe the nano-structures with 23 nm feature size. It does not require sample preparation and functions in both ambient air and liquid environments. Compared with the scientific characterization tools listed in Table S1, the simple and portable nature makes the microsphere nanoscope a favorable solution for general purpose imaging in practical fields, like hospitals, food industry, semiconductor production lines, schools and environment agencies.

Table S1 | Comparison of the imaging techniques from biological aspects.

Category	Scanning electron microscope	Transmission electron microscope	Fluorescence-based microscope (STED STROM)	Atomic force microscope	Near-field scanning microscope
Resolution	> 2 nm	> 0.2 nm	> 20 nm	> 1 nm	> 2 nm (lateral) > 20 nm (vertical)
Sample preparation & environment	Vacuum environment; Freeze/critical point drying; Conductive film coating for non-conductive samples	Sample on grid; Sample thinning; Dehydrated for bio-samples	Fluorescence labeling; Physiological treatments for bio-samples (buffer solution, temperature, CO2)	Sample on support; Physiological treatments for bio-samples (buffer solution, temperature, CO2)	Sample on support; Physiological treatments for bio-samples (buffer solution, temperature, CO2)
Limitations	Not applicable to living samples	Not applicable to living samples	Fluorescence labels required	Restricted to surfaces; Small working distance	Restricted to surfaces; Small working distance

Section 2: Photo gallery of the microsphere imaging results

Various types of semiconductor samples from the production lines are characterized with our setup, which can be successfully characterized with our microsphere nanoscope.

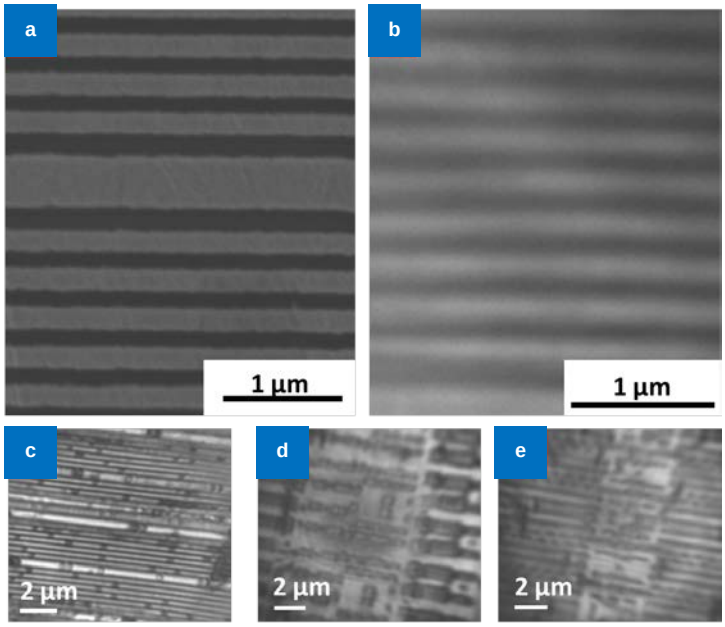

Fig. S1 | Images of various semiconductor samples. (**a**) SEM image of the CPU sample from the industry production line. The width of the nano-groove is measured to be 131 nm. Scale bar is 1 μm. (**b**) The optical image obtained by our microsphere nanoscope, which is the same CPU sample. Scale bar is 1 μm. (**c**~**e**) Different Integrated circuit samples from the production lines, scale bar is 2 μm.

Section 3: Theoretical derivation of the imaging principles

For a ball lens working in far field as presented in Fig. S2, it has the following relations according to the geometrical optics[3,4]:

$$\beta = \frac{y'}{y} = \frac{nl'}{n'l} \tag{S1}$$

$$\frac{n'}{l'} - \frac{n}{l} = \frac{n'-n}{r} \tag{S2}$$

where β is the magnification; r the radius of the ball lens; n and n' the refractive indices of the environment and the ball lens, respectively; l and l' the object and image distances from the interface, respectively; y and y' the sizes of the object and image, respectively. It should be noted that for the concave surface, r is a negative number. We can then solve S1 and S2 to rewrite the β as:

$$\beta = \frac{n}{(n'-n)\dfrac{l}{r} + n} \tag{S3}$$

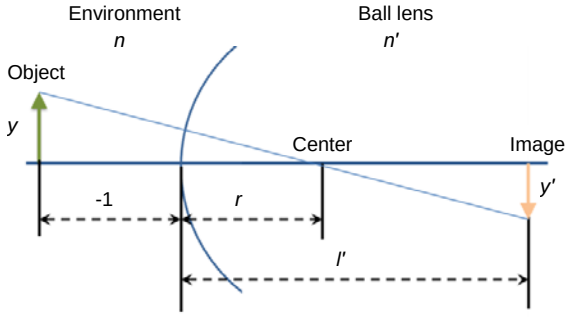

Fig. S2 | Diagram of the imaging by a ball lens.

This equation is valid for one interface. For the ball lens, it composes of two interfaces. The image of the first interface serves as the object of the second interface. Then, for the second interface, the object distance (l_2) is:

$$l_2 = l_1' - 2r \tag{S4}$$

we can substitute l_2 in the expression of the magnification to derive the contribution from the two interfaces, respectively:

$$\beta = \beta_1 \times \beta_2 \tag{S5}$$

$$\beta_1 = \frac{n_1 r}{l(n_2 - n_1) + n_1 r} \tag{S6}$$

$$\beta_2 = \frac{n_2(-r)}{l_2(n_1 - n_2) + n_2 r} \tag{S7}$$

finally, we can derive the expression of the magnification with the parameters of the ball lens and environment (please be noted that we replace the l with d to be consistent with the manuscript):

$$\beta = \frac{n_2}{2(n_2 - n_1)\dfrac{d}{r} + 2n_1 - n_2} \tag{S8}$$

this expression is valid in the domain of the geometrical optics. In our case, the diameter of the microspheres in our experiments is more than 20 μm. For the white light illumination, the upper surface can still be described by the Snell's Law. For the lower interface, a correction needs to be made on the formulas of geometrical optics as it is in the transition zone between the optical near field and far field. It is reported in various literature that the light manipulation of the lower interface is still dominated by the refraction of the microsphere interface. Computational methods are widely used to make the correction and study the magnification effect. Thus, we can define a modification factor k: [4–7]

$$\beta_2 = k \times \beta_g \tag{S9}$$

where β_g denotes the magnification calculated by the geometrical optics. As the effect of the lower interface can be well described by computational methods, we can find k by comparing the geometrical and computational results. For a ball lens, the back focusing length is defined as the distance between the focus point and the lower interface, which is used to evaluate the magnification. Then, k can be evaluated by comparing the BFL of the geometrical and computational results.

The BFL of a microsphere is calculated in geometric optics as:

$$BFL = \frac{nD}{4(n-1)} - \frac{D}{2} \tag{S10}$$

where D and n are the diameter and the refractive index of the microsphere, respectively. The first term on the right-hand side is also referred as the effective focal length (EFL) of the microsphere. For computational methods, the BFL can be found by the method presented in the literature[6].

In every experiment with the microspheres of 20 μm diameter, the microsphere is positioned at a distance of 500 nm to 1 μm above the object. We apply the theory to estimate the BFL for our experimental conditions. For example, assuming a 20 μm soda lime glass microsphere (n=1.5) is used in the high-resolution setup, it has a BFL of 5 μm. In this case, the experimentally determined working distance (500 nm to 1 μm) is well within the BFL. For this case, the key features of the imaging process are: a) the magnification is ~2.5 times as calculated with the experimental data; b) the position of this virtual image is below the surface of the object. Both these key features are verified in our experiments. We can conclude that such theory is sufficient to explain the experimental results observed in our conditions. The details are presented in the following Section 4.

Section 4: Experiments to demonstrate the virtual imaging

In the experiment demonstrated in (Video S1), a microsphere (diameter: 20 μm; silica glass) is positioned 750 nm above the sample surface. A pattern of "Ferris wheel: the Singapore Flyer" was fabricated on the sample surface as the object. The objective lens of the microscope scanned in the vertical direction and its imaging plane started from the position above the microsphere. As the objective lens moved down, it firstly observed the upper interface of the microsphere clearly (Fig. S3a). At this point, no clear image of the Singapore Flyer could be captured. The objective lens was then shifted downwards gradually. As can be seen in the process, the objective lens then observed the surface of the sample, demonstrating clearly the defects on that plane (Fig. S3b). Then, the objective lens was further shifted down. At the center of the microsphere, the virtual image of the object started to appear (Fig. S3c). The process continued until we finally reached the optimized position. At this point, the virtual image was the clearest (Fig. S3d).

It could be observed clearly that in this process, when the objective lens moved downwards, the microsphere, surface of the sample and virtual image appeared in a sequence. The virtual image was below the surface of the sample. It is solid evidence that the image captured by the objective lens was a virtual image.

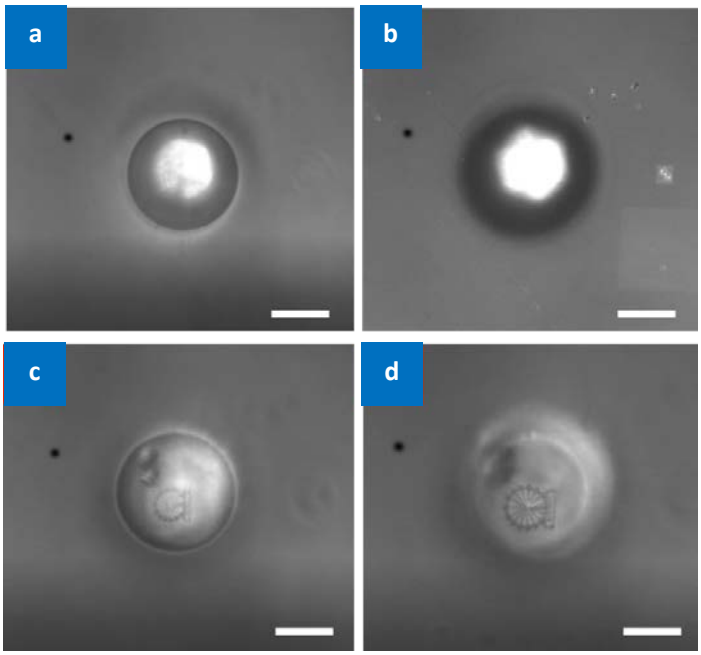

Fig. S3 | Virtual imaging process as the objective lens moves downwards to observe (**a**) the microsphere upper surface; (**b**) the sample surface; (**c**) above the plane of the virtual image and (**d**) exactly on the plane of the virtual image (scale bar is 10 μm). Imaged by a 20 μm silica microsphere compiled to the oil-immersion optical microscope (100×, NA 1.4).

Section 5: Optimization procedure for the microsphere imaging

To ensure that the objective lens captures a clear virtual image enlarged by the microsphere, the locations of the objective lens and microsphere need to be carefully aligned. This optimized distance also depends on how far away the microsphere is from the sample surface. In every experiment, there always exists an optimized distance from the microsphere to the objective lens. Simulation methods can be applied to find the optimized value between the sample surface and the microsphere. However, this method is rather tedious, as every time we need to perform the calculation for different experimental conditions.

In order to solve this problem, we have developed a straightforward imaging protocol as presented in Video S1. Firstly, we fix the location of the microsphere, so the distance between the sample and the microsphere is fixed. Then, the location of the virtual image is also fixed. In this case, we need to adjust the location of the objective lens to capture the virtual image. This can be done by scanning the objective lens in z direction (as demonstrated in the Video S1). When the contrast of the image reaches the peak value (the image becomes the clearest), the optimized location of the objective lens is found. This operation is rather simple and fast (it takes tens seconds to find the optimized location).

For the integrated system presented in Fig. 3, the mechanism to find out the optimized locations is a bit different. For this case, we also develop an imaging protocol by first compiling the microsphere to the objective lens, so the distance between the microsphere and the objective lens is fixed. For this optical system, there exists an optimized observation position for the object, similar to the conventional optical microscope system. Secondly, we perform the standard operation procedure as same as the conventional optical microscope by scanning the object in z direction to locate the optimized location for clear imaging.

Section 6: Real-time imaging results

Another advantage of our microsphere nanoscope is its capability to perform real-time observation. We have recorded the characterization processes of the nano-dots, nano-rose and a semiconductor testing chip to demonstrate the capability to perform the dynamic characterization (Video S2~S4). Video S2 demonstrates the characterization process of the nano-dots' sample. In this experiment, the optimized Z location for the microsphere and the objective lens is found via the methods presented in Supplementary information Section 3. Then, the microsphere is scanned in *XY* plane. As demonstrated in the video, the nano-dots' pattern is clearly enlarged by the microsphere. The gaps between the nano-dots can be distinguished clearly. This imaging process preserves most advantages of the conventional microscope. It can scan through a large sample surface and monitor the sample dynamically.

Similarly, the characterization process of the nano-rose is also demonstrated in Video S3. The operation procedure is the same as the Video S2. This process proves the nanoscope's capability to observe complicated patterns. The gaps in the nano-rose pattern can be clearly observed by the microsphere. In Video S2 and Video S3, the background color is set to be white to better highlight the imaging results of the microsphere. For the semiconductor testing sample presented in Fig. 1c, similar characterization is performed. The results are recorded in Video S4. No post-image processing technique is applied to the raw image to improve the quality. Certainly, the application of post-imaging processing technologies can further reduce the aberration and improve the imaging quality greatly, which demonstrates the potential for further improvement. This video clip shows that our method can observe the nano-patterns clearly. The operation of the microsphere nanoscope is almost as same as the conventional optical microscope. This indicates that the microsphere nanoscope is compatible with most of the conventional microscopes as it offers a straight-forward and cost-efficient solution.

Section 7: Line-cut analysis for nano-dots' image in Fig. 3c

To better analyze the image of the nano-dots' pattern, the line cut is taken in Fig. 3c. The light intensity of every position is normalized to the intensity value corresponding to the white color. Then, the normalized intensity at every position is plotted respect to *Y* axis. The two nano-dots can be clearly distinguished as shown in this figure. Two local minimum values are shown clearly, which corresponds to the center of the neighboring nano- dots (As the nano-dots are presented by dark color in the image, the intensity value is lower compared to other locations). It is solid evidence that the microsphere provides the enlarged virtual image of the nano-dots. The virtual image enlarged by the microsphere is then captured by the objective lens.

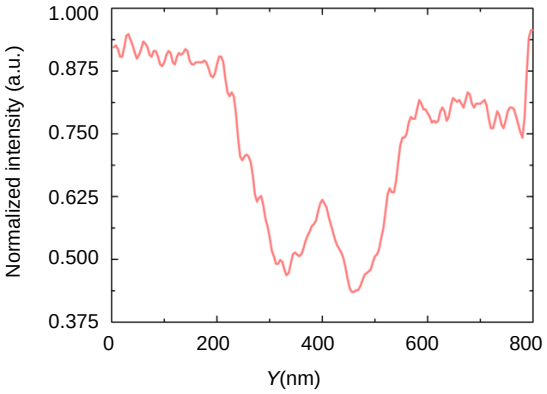

Fig. S4 | Line-cut analysis for the nano-dot image.

Supplementary information references

1. Dufrêne Y F, Ando T, Garcia R, Alsteens D, Martinez-Martin D, *et al*. Imaging modes of atomic force microscopy for application in molecular and cell biology. *Nat Nanotechnol* **12**, 295–307 (2017).
2. Dürig U, Pohl D W, Rohner F. Near‐field optical‐scanning microscopy. *J Appl Phys* **59**, 3318–3327 (1986)
3. Born M, Wolf E. *Principles of optics ; electromagnetic theory of propagation, interference, and diffraction of light* (Pergamon Press, 1975).
4. Soroko L M. *Meso-optics : foundations and applications* (World Scientific, 1996).
5. Wang Z B, Guo W, Li L, Luk'yanchuk B, Khan A *et al*. Optical virtual imaging at 50 nm lateral resolution with a white-light nanoscope. *Nat Commun* **2**: 218 (2011).
6. Yang H, Trouillon R, Huszka G, Gijs M A M. Super-resolution imaging of a dielectric microsphere is governed by the waist of its photonic nanojet. *Nano Lett* **16**, 4862–4870 (2016).
7. Astratov V N, Abolmaali F, Brettin A, Allen K W, Maslov A V *et al.* Label-free nanoscopy with contact microlenses : super-resolution mechanisms and limitations. In *2016 18th International Conference on Transparent Optical Networks* (2016); http://doi.org/10.1109/ICTON.2016.7550529.